Choice of dipole operator gauge in time-dependent *R*-matrix theory

2010 J. Phys. B: At. Mol. Opt. Phys. 43 095603

(http://iopscience.iop.org/0953-4075/43/9/095603)

J. Phys. B: At. Mol. Opt. Phys. **43** (2010) 095603 (10pp) doi:10.1088/0953-4075/43/9/095603

Choice of dipole operator gauge in time-dependent *R*-matrix theory

S Hutchinson, M A Lysaght and H W van der Hart

Centre for Theoretical Atomic, Molecular and Optical Physics, School of Mathematics and Physics, Queen's University Belfast, Belfast BT7 1NN, UK

E-mail: shutchinson06@qub.ac.uk

Received 15 December 2009, in final form 19 March 2010
Published 15 April 2010
Online at stacks.iop.org/JPhysB/43/095603

Abstract

We investigate multi-photon ionization of helium using the time-dependent *R*-matrix method in order to assess the best choice of gauge for the description of the laser field when the system under investigation is a multi-electron system. Ionization probabilities are obtained using the length gauge and the velocity gauge and various He basis sets, when a minimum of three or four photons need to be absorbed to achieve ionization. The probabilities are found to converge for both gauges as the number of orbitals used in the basis set increases, but they are more consistent in the length gauge. Ionization probabilities can be compared to those derived from other theoretical calculations. Agreement is within 10% when ionization requires absorption of at least three photons, but the differences increase to 20–50% when absorption of four photons is required. Analysis of the multi-photon matrix elements provides further evidence for better consistency in the length gauge than the velocity gauge when high-lying states are excluded from the calculations, which is, at present, unavoidable for a multi-electron system.

(Some figures in this article are in colour only in the electronic version)

1. Introduction

One of the main challenges in computational atomic physics is the description of multi-electron dynamics in intense laser fields. This area is of increasing relevance due to developments in laser physics allowing high intensity pulses to be generated for ever shorter wavelengths [1, 2]. The accurate description of a multi-electron field-free atomic system requires substantial computational resources that increase exponentially with the number of electrons. The problem is even more demanding when the system is in a laser field which breaks the isotropy of space so that the total angular momentum is no longer conserved. Computational limits thus restrict the size of the system being considered or the accuracy of the description.

Over the last two decades, great progress has been made in the description of two-electron systems in intense laser fields. One of the most advanced approaches in this area is the so-called HELIUM approach of Parker, Taylor and co-workers which solves the laser-driven two-electron problem through direct numerical integration of the full-dimensional time-dependent Schrödinger equation [3]. This method has proved to be highly successful in accurately describing He irradiated by an intense 390 nm laser field [4]. For a general multi-electron atom or ion, however, very few theoretical methods exist that are capable of describing the response of a target atom or ion irradiated by an intense laser pulse, and those that do typically employ a single active electron (SAE) approximation. The SAE approximation assumes that only one electron is active in the system which limits the ability to describe multi-electron effects that require more than one active electron, such as electron correlation and exchange interactions in particular.

Recently, first attempts have been made in the *ab initio* time-dependent investigation of atomic systems in intense laser fields for a general multi-electron system. One such method is the recently developed time-dependent *R*-matrix (TDRM) theory which is a non-perturbative *ab initio* method capable of describing a general multi-electron atom or ion in an intense time-dependent light field [5–8]. Two different versions of TDRM theory have been developed: one type of approach in which dynamics is restricted to an enlarged internal region [5, 7, 8] and one in which space is separated into an internal region and an external region [6]. The latter method is of current interest. The method has been described in detail elsewhere [9], and its success in describing atomic

interactions has been demonstrated in recent studies of ultra-fast laser-driven excitation dynamics in Ne [6] and ultra-fast multi-electron dynamics in a C^+ ion [10, 11].

One of the key questions which has to be considered in applications of time-dependent *R*-matrix theory is the choice of gauge in which to describe the laser fields. If exact atomic wavefunctions are used for all states, the choice of gauge is irrelevant as the same result will be obtained regardless. Unfortunately, for a general multi-electron atom or ion, it becomes impractical to use exact (or nearly exact) wavefunctions for all states due to the scale of the calculations required. With an approximate wavefunction, the choice of gauge, and specifically how quickly convergence is achieved with respect to the basis used, becomes an important factor in the overall calculation.

The choice of gauge is not trivial, since different areas of theoretical atomic physics have different preferences for the choice of gauge. The dipole operator appearing in the description of the interaction between the laser field and the electrons is frequently described in the length gauge for atomic structure calculations, whereas it is primarily described in the velocity gauge for strong field studies. On the other hand, atomic structure calculations routinely include multi-electron excitations, whereas strong-field studies are currently limited to at most two active electrons. Previous studies of gauge choice for strong field calculations have demonstrated conclusively that the velocity gauge is the preferred choice for single-active electron studies [12, 13]. However, this analysis cannot be trivially extended to a general multi-electron system. Indeed, a previous investigation into ultra-fast multi-electron dynamics in argon using the time-dependent *R*-matrix method [5] has already successfully employed the length gauge. In this case the length gauge was preferred due to intermediate states in which three or four electrons are excited. The influence of these intermediate states, which cannot be described accurately, is significantly larger in velocity-gauge calculations than in length gauge ones. It is therefore of importance to demonstrate and evaluate how the choice of gauge affects the numerical outcomes.

The non-trivial nature of the choice of gauge can be appreciated further by considering other approaches. One of the most successful methods for the description of general atoms in intense laser fields is the *R*-matrix Floquet method [14], which uses both the length and velocity gauges depending on the distance from the nucleus. The *R*-matrix Floquet approach further employs the acceleration frame to define the proper asymptotic solutions at very large distances. Another approach proposed by Robicheaux *et al* [15] uses a more complex smoothly varying mixed gauge. This mixed gauge is chosen to approach the most relevant gauge for the distance from the nucleus, with the change between each occurring smoothly over a range of distances.

To assess the choice of gauge, we investigate in the present paper the suitability of the length and velocity forms of the dipole operator in the time-dependent *R*-matrix approach for the description of multi-photon ionization of He irradiated by an intense laser field. Helium was chosen as it provides one of the simplest multi-electron systems. This simplicity allows the comparison of the length and velocity gauges for basis sets which can be varied in a systematic manner. In addition, accurate theoretical ionization rates and cross-sections have been presented for three- and four-photon ionization [16, 17], which can provide an independent measure of the accuracy of the calculations.

The outline of the paper is as follows; we start by giving a brief overview of the time-dependent *R*-matrix approach in section 2. We then present in section 3 an overview of ionization probabilities for three- and four-photon ionization of He, followed by a discussion and interpretation of these results.

2. Methodology

In this section we give an overview of the time-dependent *R*-matrix method, which is employed throughout this paper. Thorough overviews of this method for 1D single electron studies [18] and for atomic studies [9] have been published previously and may be consulted for further details. The recent applications of the method to atomic systems [9] describe the dipole operator in the length gauge. However, when the method was originally proposed for a 1D single-electron problem [18], a velocity-gauge description of the dipole operator was used instead. Since we are interested in the comparison between the length- and velocity-gauge descriptions of the dipole operator, the overview given in this section will be general enough to be applicable in each case, with occasional comments on differences that arise in the theoretical formulation of each.

The TDRM method attempts to find a solution to the time-dependent Schrödinger equation (TDSE) for a general $(N + 1)$-electron atom or ion interacting with a light field. Throughout this paper the light field is assumed to be spatially homogeneous and linearly polarized. Through the use of the unitary Cayley form of the time evolution operator $\exp(-it\,H(t))$, the TDSE may be expressed in a form that allows the use of a Crank–Nicolson scheme as follows:

$$\left(H\left(t_{q+\frac{1}{2}}\right) - E\right)\Psi(\mathbf{X}_{N+1}, t_{q+1}) = \Theta(\mathbf{X}_{N+1}, t_q), \tag{1}$$

where

$$\Theta(\mathbf{X}_{N+1}, t_q) = -\left(H\left(t_{q+\frac{1}{2}}\right) + E\right)\Psi(\mathbf{X}_{N+1}, t_q). \tag{2}$$

In equations (1) and (2), $\mathbf{X}_{N+1} \equiv \mathbf{x}_1, \mathbf{x}_2, \ldots, \mathbf{x}_{N+1}$, where $\mathbf{x}_i \equiv \mathbf{r}_i\sigma_i$ are the space and spin coordinates of the ith electron and $H\left(t_{q+\frac{1}{2}}\right)$ is the time-dependent Hamiltonian at the midpoint of times t_q and t_{q+1}. The imaginary energy is defined by the time step $\Delta t = t_{q+1} - t_q$ and is given by $E \equiv 2\mathrm{i}\Delta t^{-1}$. The Hamiltonian can be written in the form

$$H(t) = H_{N+1} + H_{\mathrm{int}}(t), \tag{3}$$

where H_{N+1} is the standard $(N + 1)$ electron Hamiltonian in the absence of an external field and $H_{\mathrm{int}}(t)$ represents the laser interaction term. In the length gauge, $H_{\mathrm{int}}(t)$ is given as

$$H_{\mathrm{int}}(t) = \sum_{i=1}^{N+1} \mathbf{E}(t) \cdot \mathbf{r}_i, \tag{4}$$

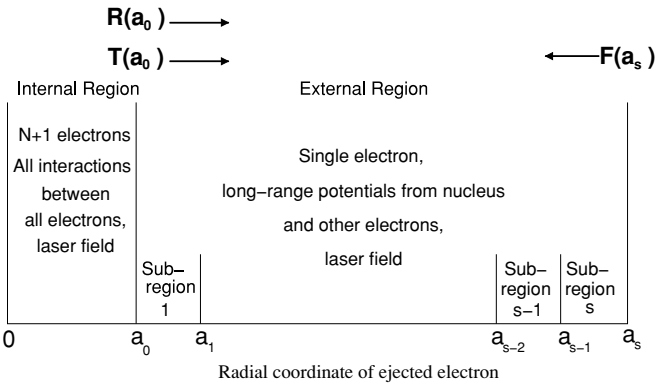

Figure 1. Partition scheme for the configuration space.

and in the velocity gauge as

$$H_{\rm int}(t) = \frac{1}{c}\sum_{i=1}^{N+1}\mathbf{A}(t)\cdot\mathbf{p}_i. \tag{5}$$

Following the standard R-matrix method [19], configuration space is partitioned into an internal region and an external region, as shown in figure 1. The internal region contains all $(N+1)$ electrons, and exchange and correlation effects are fully taken into account. In the external region, in which there is one ejected electron, exchange with the inner electrons is considered negligible. The internal and external regions are linked at a boundary $r = a_0$. The outer limit of the external region, $r = a_s$, is chosen large enough so that the outgoing wavepacket does not reach it before the end of the propagation. A suitable choice of a_s is crucial to ensure that this condition is physically correct when imposed as a boundary condition.

When considering the matrix equation (1) in the internal region, we note that the Hamiltonian used is not Hermitian due to the kinetic energy operator. Similar to standard R-matrix theory [19], this is complemented through the addition of a Bloch operator $\mathcal{L}_1$ such that $(H_{N+1} + \mathcal{L}_1)$ is Hermitian. The velocity-gauge theory differs slightly in that, while $\mathcal{L}_1$ is still needed, there is now also a second non-Hermitian term present in the Hamiltonian used in (1) due to the laser interaction term $\frac{1}{c}\sum_{i=1}^{N+1}\mathbf{A}\cdot\mathbf{p}_i$. A second Bloch operator $\mathcal{L}_2$ is added in the same way to the Hamiltonian to ensure Hermicity in the internal region as detailed by Dörr *et al* [20]. Equation (1) is then rewritten in the following form:

$$\Psi = \left(\frac{1}{H+\mathcal{L}-E}\right)(\mathcal{L}\Psi + \Theta), \tag{6}$$

where for notational simplicity we have omitted the arguments in H,Ψ and Θ. The Bloch operator term $\mathcal{L}$ represents the sum of all relevant Bloch operators.

In the internal region the wavefunction $\Psi(\mathbf{X}_{N+1}, t_{q+1})$ is expanded in terms of a completely antisymmetric R-matrix basis $\psi_k(\mathbf{X}_{N+1})$ and we use the same methods of analysis as a recently developed R-matrix inner region approach [5], which produces dipole matrix elements for both the length gauge and the velocity gauge, to set up the linear equations given by (1). Using a linear solver at each time step we determine the R-matrix, $\mathbf{R}$, at the boundary $r = a_0$ with elements defined as [9]

$$R_{pp'}(E) = \frac{1}{2a_0}\sum_{kk'}\omega_{pk}\left(\frac{1}{H+\mathcal{L}-E}\right)_{kk'}\omega_{p'k'}, \tag{7}$$

where p, $p' = 1, \ldots, n$ and where the surface amplitudes ω_{pk} are defined by

$$\omega_{pk} = \left\langle\bar{\Phi}_{p\gamma}r_{N+1}^{-1}\middle|\psi_k\right\rangle'_{r_{N+1}=a_0}, \tag{8}$$

where $p = 1, \ldots, n$ and $k = 1, \ldots, n_t$. We also determine an inhomogeneous T-vector, $\mathbf{T}$, at the same boundary, defined as

$$T_p(a_0) = \sum_{kk'}\omega_{pk}\left(\frac{1}{H+\mathcal{L}-E}\right)_{kk'}S_k, \tag{9}$$

where $p = 1, \ldots, n$ and S_k is the projection defined as

$$S_k = \langle\psi_k \mid \Theta\rangle, \tag{10}$$

where $k = 1, \ldots, n_t$. In each case n represents the number of retained channel functions $\bar{\Phi}_{p\gamma}$, which are formed by coupling the residual atom or ion states Φ_i with angular and spin functions of the ejected electron [9], and n_t represents the total number of linearly independent basis functions ψ_k retained in the close coupling expansion of the R-matrix basis functions presented in [9]. For both the R-matrix and T-vector we note that gauge dependence is contained in the Bloch operators. At this point, we cannot find the wavefunction $\Psi(\mathbf{X}_{N+1}, t_{q+1})$ without either restricting the configuration space to the internal region only, as in [5], or extending our analysis to the external region.

Crucial to the solution of (1) in the internal region is linking the internal and external regions at the boundary $r = a_0$, thus ensuring that the solution is physically meaningful. This is achieved by projecting (6) onto the channel functions $\bar{\Phi}_{p\gamma}$ and evaluating the resulting expression at this boundary giving the following matrix equation:

$$\mathbf{F}(a_0) = \mathbf{R}a_0\bar{\mathbf{F}}(a_0) + \mathbf{T}(a_0), \tag{11}$$

where the reduced radial wavefunctions are defined as

$$F_p(a_0) = \left\langle\bar{\Phi}_{p\gamma}r_{N+1}^{-1}\middle|\Psi\right\rangle'_{r_{N+1}=a_0}. \tag{12}$$

The prime on the matrix elements indicates integration over the space and spin coordinates of all $(N+1)$ electrons except the radial coordinate r_{N+1} of the ejected electron. Analytic continuations of these reduced radial functions exist in the external region and as such (11) can be used to link the internal and external regions. Finally we note that the modified derivative functions $\bar{F}_p(a_0)$ arise entirely due to the Bloch operators used in (6) and their definition will vary between the length gauge and the velocity gauge.

While the R-matrix and T-vector in (11) are obtained from analysis of the internal region alone, the modified derivative functions $\bar{F}_p(a_0)$ remain unknown. Thus, the modified derivative functions must be determined from the solution of the external region before we can determine the internal region wavefunction $\Psi(\mathbf{X}_{N+1}, t_{q+1})$ [9].

In order to solve (1) in the external region, we expand the wavefunction Ψ in terms of the reduced radial functions $F_p(r)$

which represent the motion of an electron in the pth channel as follows:

$$\Psi(\mathbf{X}_{N+1}, t_{q+1}) = \sum_{p=1}^{n} \bar{\Phi}_{p\gamma}(\mathbf{X}_N; \hat{\mathbf{r}}_{N+1}\sigma_{N+1}) r_{N+1}^{-1} F_p(r_{N+1}), \tag{13}$$

where $\bar{\Phi}_{p\gamma}$ are the channel functions from before. The subscript p represents the channel quantum numbers L, i and $\gamma = \alpha S M_L M_S \pi$.

To obtain a solution for the wavefunction of the ejected electron in the external region we substitute (13) into (1) and project onto the channel functions $\bar{\Phi}_{p\gamma}$ obtaining coupled second-order differential equations which can be expressed in matrix form as

$$(\mathbf{H}_{\text{ext}} - E\mathbf{I})\mathbf{F}(r) = \theta(r), \tag{14}$$

where the Hamiltonian $\mathbf{H}_{\text{ext}}$ is defined as

$$\mathbf{H}_{\text{ext}} = -\frac{1}{2}\left(\mathbf{I}\frac{\mathrm{d}^2}{\mathrm{d}r^2} + \mathbf{V}(r) - 2\mathbf{W}(r) + \mathbf{k}^2\right). \tag{15}$$

Here, $\mathbf{V}(r)$ represents the combined nuclear and centrifugal potential matrix, $\mathbf{W}(r)$ represents the long-range potential matrix coupling the channels and $\mathbf{k}^2$ can be expressed in terms of the diagonal energy eigenvalue matrix $\mathbf{E}_n$ of the residual N-electron ion by the equation $\mathbf{k}^2 = -2\mathbf{E}_n$. We note that (15) applies to both gauge descriptions; however, the long-range potential matrix $\mathbf{W}(r)$ is not the same in each case. Explicit forms of $\mathbf{W}(r)$ may be found in [9] for the length gauge and [14] may be used to derive an explicit form for the velocity gauge. Finally, the inhomogeneous term $\theta(r)$ in (14) is defined for a single channel as

$$\theta_p(r) = \left\langle \bar{\Phi}_{p\gamma}(\mathbf{X}_N; \hat{\mathbf{r}}_{N+1}\sigma_{N+1}) r_{N+1}^{-1} \middle| \Theta_{\text{out}} \right\rangle, \tag{16}$$

where

$$\Theta_{\text{out}} = -(\mathbf{H}_{\text{ext}} + E)\mathbf{F}. \tag{17}$$

We now note that the external region is further partitioned into s sub-regions, as shown in figure 1. Similar to the internal region, Hermicity of the Hamiltonian in each subregion is ensured through the addition of the Bloch operators $\mathcal{L}_s$. Thus, (14) in the sth subregion may be expressed as

$$(\mathbf{H}_{\text{ext}} + \mathcal{L}_s - E\mathbf{I})\mathbf{F}(r) = \mathcal{L}_s\mathbf{F}(r) + \theta(r). \tag{18}$$

The formal solution to (18) in the sth subregion may then be written as

$$\mathbf{F}(r) = 2\int_{a_{s-1}}^{a_s} \mathbf{G}_s(r, r')\mathcal{L}_s\mathbf{F}(r')\,\mathrm{d}r' + \mathbf{J}(r), \tag{19}$$

where

$$\mathbf{J}(r) = 2\int_{a_{s-1}}^{a_s} \mathbf{G}_s(r, r')\theta(r')\,\mathrm{d}r', \tag{20}$$

where the Green's function $G_s(r, r')$ is the solution of

$$(\mathbf{H}_{\text{ext}} + \mathcal{L}_s - E\mathbf{I})\mathbf{G}_s(r, r') = \tfrac{1}{2}\mathbf{I}\delta(r - r'). \tag{21}$$

We use a spectral representation of the Green's function in equations (19) and (20) [9], where we use a basis of B-splines and solve a system of linear equations in each sub-region.

Evaluation of (21) at $r = a_{s-1}$ and $r = a_s$ results in the following equations that allow the outward propagation of the R-matrix and T-vectors from the boundary at $r = a_{s-1}$ to $r = a_s$ [9]:

$$a_s\mathbf{R}_s = \mathbf{G}_s(a_s, a_s) - \mathbf{G}_s(a_s, a_{s-1}) \times [\mathbf{G}_s(a_{s-1}, a_{s-1}) + a_{s-1}\mathbf{R}_{s-1}]^{-1}\mathbf{G}_s(a_{s-1}, a_s) \tag{22}$$

and

$$\mathbf{T}(a_s) = \mathbf{J}(a_s) + \mathbf{G}_s(a_s, a_{s-1})[\mathbf{G}_s(a_{s-1}, a_{s-1}) + a_{s-1}\mathbf{R}_{s-1}]^{-1}(\mathbf{T}(a_{s-1}) - \mathbf{J}(a_{s-1})). \tag{23}$$

Finally, we obtain the following equation for the inward propagation of the F-vector from a boundary $r = a_s$ to $r = a_{s-1}$ using the R-matrix, T- and F-vectors at $r = a_s$ [9]:

$$\mathbf{F}(a_{s-1}) = a_{s-1}\mathbf{R}_{s-1}[\mathbf{G}_s(a_{s-1}, a_{s-1}) + a_{s-1}\mathbf{R}_{s-1}]^{-1} \times \left[\mathbf{G}_s(a_{s-1}, a_s)a_s^{-1}\mathbf{R}_s^{-1}(\mathbf{F}(a_s) - \mathbf{T}(a_s)) + \mathbf{G}_s(a_{s-1}, a_{s-1})a_{s-1}^{-1}\mathbf{R}_{s-1}^{-1}\mathbf{T}(a_{s-1}) + \mathbf{J}(a_{s-1})\right]. \tag{24}$$

The outward propagators (22) and (23) are used first to propagate the R-matrix and T-vectors calculated at the boundary $r = a_0$ from the analysis of the internal region to the outer limit of the external region. We then use the inward propagator (24) in conjunction with the condition that the ejected electron wavepacket does not reach the outer boundary and (19) to determine the F-vector at every point of the external region. From the F-vector, we then calculate the wavefunction $\Psi(\mathbf{X}_{N+1}, t_{q+1})$ using (19) for the external region and (11) to determine the internal region wavefunction.

In this paper we are primarily interested in the ionization process. For this purpose, we consider the target to be ionized when an electron is no longer under the direct influence of the individual electrons and nucleus of the target. In the present calculations, this is considered to occur at the moment an electron enters the external region, where the frequencies of the laser field have been chosen such that there is no major influence from high-lying Rydberg states. Thus, we consider the probability of ionization to be equivalent to the probability of an electron being present in the external region.

3. Application to helium

3.1. Description of He and fields used in the calculations

Our investigation considers a He atom ionized by a single ultra-short light pulse, with primary interest on the choice of gauge for the dipole operator and how it affects the obtained ionization rates with respect to the size and complexity of the description of He. The TDRM method described in the previous section is applied for both the length- and velocity-gauge descriptions of the dipole operator. A comparison between each gauge is carried out for two different frequencies, corresponding to ionization requiring absorption of a minimum of three, or four, photons and for different basis set descriptions of He. Before presenting the ionization probabilities, we first discuss the description of He.

Since our interest is focused on how the choice of gauge is connected to the detail used to describe He, several basis sets are employed. However, they have several common properties. For all calculations, we use an internal region radius of 30 au with the R-matrix and T-vector in the external region being

propagated outwards to a distance of 453 au. The internal region is considered large enough to contain the residual ion for each basis set considered, with the radius kept constant to ensure that changes in results are due entirely to changes in the basis set used. Each external region sector is 3.0 au in width and contains 40 B-splines of order $k = 9$ for each channel. In all cases the set of continuum orbitals contains at least 50 continuum functions for each available angular momentum of the continuum electron, with a maximum total angular momentum $L_{\max} = 7$. Some calculations were also performed using $L_{\max} = 9$; however, these were found to produce nearly identical results to the calculations with $L_{\max} = 7$.

The various descriptions of He differ in the states included in the basis sets for He and He^+. The He basis in the internal region consists of a set of pseudo-continuum orbitals, built from a complete set of B-splines, attached to a set of He^+ final states. The He basis set is then varied by varying the set of He^+ final states. The most basic model used includes only the He^+ 1s state, with more extensive models including the He^+ 2s and 2p states and the most extensive model using real He^+ states up to and including 3s, 3p and 3d. However, we can choose the kind of orbital we want for these excited states of He^+. We are interested in ionization leaving the He^+ ion in the 1s state therefore, we can also use pseudo-orbitals $\overline{2s}$, $\overline{2p}$, $\overline{3s}$, $\overline{3p}$ and $\overline{3d}$ rather than the real orbitals. These pseudo-orbitals could provide a better description of the changes to the He^+ 1s ground state during the laser pulse, and hence a better description of the ionization process. The choice of basis sets and pseudo-orbitals can be made in several ways. We have chosen to include He^+ bases consisting of 1s only, a 1s,2s,2p basis and a 1s,$\overline{2s}$,$\overline{2p}$ basis. Inclusion of the $n = 3$ orbitals gives more combinations: a 1s,2s,2p,3s,3p,3d basis and a 1s,$\overline{2s}$,$\overline{2p}$,$\overline{3s}_1$,$\overline{3p}_1$,$\overline{3d}_1$ basis. Finally we include two basis sets incorporating real $n = 2$ orbitals and $n = 3$ pseudo-orbitals, 1s,2s,2p,$\overline{3s}_1$,$\overline{3p}_1$,$\overline{3d}_1$ and 1s,2s,2p,$\overline{3s}_2$,$\overline{3p}_2$,$\overline{3d}_2$. The functional form of the radial component of our pseudo-orbitals is given by Slater-type orbitals of the form

$$\overline{nl}_{n'} = \sum_{i=l+1}^{n} c_i r^i \, \mathrm{e}^{-2r/n'}, \tag{25}$$

where the subscript n' is used to denote the exponential behaviour of the pseudo-orbital. The value of the coefficients c_i is determined uniquely (apart from overall sign) by $c_i = 0$ for $i < l + 1$, orthogonality and normalization conditions.

We consider a laser frequency $\omega = 0.33$ au, corresponding to an energy for which a minimum of three photons are required to ionize He and a laser frequency $\omega = 0.24$ au, corresponding to an energy for which a minimum of four photons are required to ionize He. While we acknowledge that higher order processes, involving the absorption of more than the minimum required number of photons, are possible at these frequencies, for clarity in further discussion these ionization processes will be referred to as a three- and four-photon process respectively. In each case the laser has a peak intensity of 2×10^{13} W cm^{-2} and consists of a 3-cycle $\sin^2$ ramp-on of the electric field, followed by six cycles at peak intensity, finishing with a 3-cycle $\sin^2$ ramp-off. To ensure consistency between each gauge, the vector potential is calculated by integration of the previously stated electric field. The resulting laser pulses have durations of 5.53 fs and 7.60 fs in the $\omega = 0.33$ au and $\omega = 0.24$ au cases respectively. In each case the system was allowed to freely evolve for approximately 5 fs beyond the end of the laser pulse. The total ionization probability is determined by integration of the ejected electron probability density over the entire external region. We will first show the outcomes for each of the four sets of calculations, and compare the results in detail afterwards.

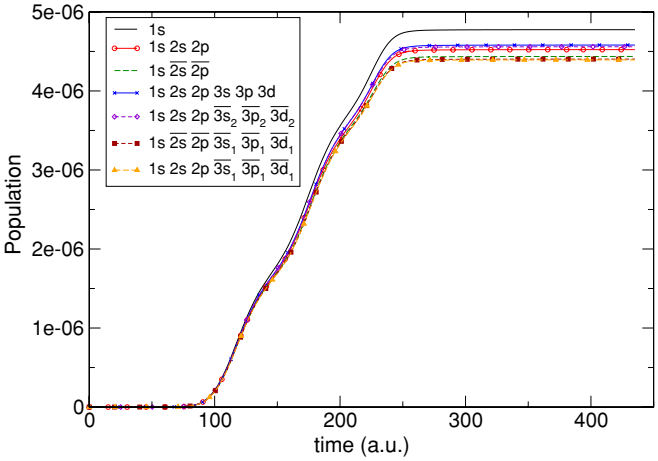

Figure 2. Population of the external region ($r > 30$ au) for various basis sets using the length gauge and a pulse frequency of $\omega = 0.33$ au with six cycles at a peak intensity of 2×10^{13} W cm^{-2}. The basis sets used are defined in terms of the states of He^+ included. Shown are basis sets including the real (solid lines) He^+ orbitals 1s, 1s 2s 2p (circles) and 1s 2s 2p 3s 3p 3d (crosses) along with those involving pseudo-states of He^+ (dashed lines) 1s $\overline{2s}$ $\overline{2p}$, 1s 2s 2p $\overline{3s}_1$ $\overline{3p}_1$ $\overline{3d}_1$ (solid triangles), 1s 2s 2p $\overline{3s}_2$ $\overline{3p}_2$ $\overline{3d}_2$ (diamonds), 1s $\overline{2s}$ $\overline{2p}$ $\overline{3s}_1$ $\overline{3p}_1$ $\overline{3d}_1$ (solid squares). Here, a subscript on an orbital indicates the exponential behaviour of the orbital.

3.2. Results

Figure 2 shows the evolution of the external region population in time for a laser frequency $\omega = 0.33$ au using the length-gauge description of the dipole operator. The final ionization probability obtained is consistent across the range of basis sets used, with a ratio between the highest and lowest probabilities of 1.09. The most significant deviation occurs when we include only the He^+ 1s orbital in our basis set, which produces the highest result in figure 2. Finally, basis sets which include pseudo-orbitals with an exponential decay similar to the 1s orbital tend to produce the lowest ones in figure 2. Numerical values for the final ionization probabilities are given in table 1.

The ionization probabilities obtained using the velocity-gauge description of the dipole operator for a laser frequency of $\omega = 0.33$ au are shown in figure 3. Although these probabilities converge onto the same result as the length gauge, they appear significantly more sensitive with respect to the He^+ orbitals included in the basis set. Consequently the final results are much more inconsistent, with a ratio between the highest and lowest probabilities of 1.7. Again the population obtained in the calculation in which only the 1s state of He^+ is

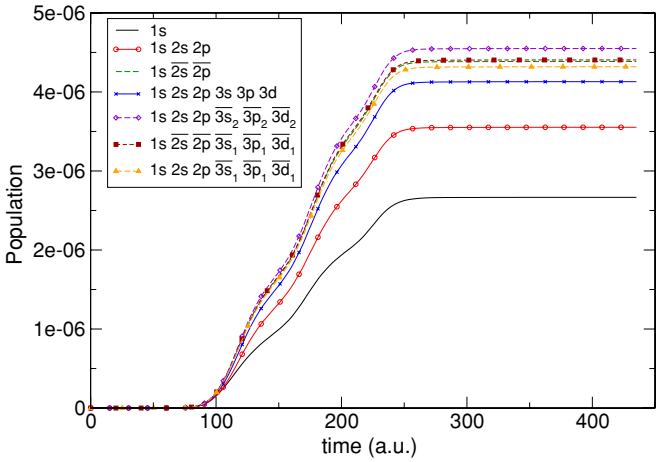

Figure 3. Population of the external region for various basis sets using the velocity gauge with a laser frequency of $\omega = 0.33$ au for six cycles at a peak intensity of 2×10^{13} W cm^{-2}. Details on the basis sets used are given in the caption to figure 2.

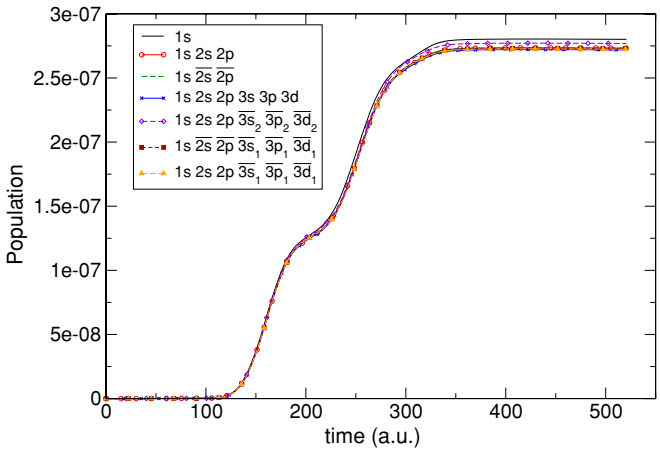

Figure 4. Population of the external region for the length gauge using a pulse frequency of $\omega = 0.24$ au for six cycles at a peak intensity of 2×10^{13} W cm^{-2}. Details on the basis sets used are given in the caption to figure 2.

Table 1. Final outer-region populations obtained for various basis sets using a laser pulse with a frequency $\omega = 0.33$ au for six cycles at a peak intensity of 2×10^{13} W cm^{-2} with both a length- and velocity-gauge description of the dipole operator.

Basis set	Length gauge 10^{-6}	Velocity gauge 10^{-6}	Ratio
1s	4.775	2.666	0.5583
1s 2s 2p	4.523	3.553	0.7855
1s $\overline{2s}$ $\overline{2p}$	4.436	4.386	0.9886
1s 2s 2p 3s 3p 3d	4.581	4.130	0.9016
1s 2s 2p $\overline{3s}_2$ $\overline{3p}_2$ $\overline{3d}_2$	4.559	4.550	0.9978
1s 2s 2p $\overline{3s}_1$ $\overline{3p}_1$ $\overline{3d}_1$	4.393	4.318	0.9830
1s $\overline{2s}$ $\overline{2p}$ $\overline{3s}_1$ $\overline{3p}_1$ $\overline{3d}_1$	4.403	4.405	1.000

Table 2. Final outer-region populations obtained for various basis sets using a laser pulse with a frequency $\omega = 0.24$ au for six cycles at a peak intensity of 2×10^{13} W cm^{-2} with both a length- and velocity-gauge description of the dipole operator.

Basis set	Length gauge 10^{-7}	Velocity gauge 10^{-7}	Ratio
1s	2.801	10.45	3.731
1s 2s 2p	2.733	2.574	0.9418
1s $\overline{2s}$ $\overline{2p}$	2.733	2.758	1.009
1s 2s 2p 3s 3p 3d	2.719	2.147	0.7898
1s 2s 2p $\overline{3s}_2$ $\overline{3p}_2$ $\overline{3d}_2$	2.769	2.457	0.8873
1s 2s 2p $\overline{3s}_1$ $\overline{3p}_1$ $\overline{3d}_1$	2.724	2.760	1.013
1s $\overline{2s}$ $\overline{2p}$ $\overline{3s}_1$ $\overline{3p}_1$ $\overline{3d}_1$	2.729	2.706	0.9914

included lies furthest from any other result obtained using the same frequency and gauge. However, in the velocity-gauge description, it provides a much lower ionization probability than calculations with additional He^+ basis orbitals, as opposed to the length gauge where it is slightly higher than the other results. Numerical values for the final ionization probabilities are also given in table 1.

In the case of three-photon ionization of He by a laser pulse with frequency $\omega = 0.33$ au and intensity 2×10^{13} W cm^{-2}, we can compare the present calculations in detail with earlier time-independent *R*-matrix Floquet calculations by van der Hart and Bingham [16]. These *R*-matrix Floquet calculations provided three-photon ionization rates for He in the frequency region between 0.31 and 0.44 au. These ionization rates were found to be in good agreement with perturbation theory calculations [17]. For the present purpose, we compare the estimated ionization probability derived from the ionization rates calculated using the *R*-matrix Floquet method for a basis set that includes only the 1s, 2s and 2p states of He^+ with the corresponding result obtained in table 1 using the TDRM method. The ionization probability determined from the time-independent method was found to be 4.08×10^{-6}, which is approximately 10% lower than the result obtained using the length gauge, and approximately 15% higher than the velocity-gauge calculation. Ultimately both gauges converge to a final ionization probability in the region of 10% higher than that is given from the time-independent calculation. This is quite good overall agreement between the two methods, since a relatively short pulse is used in the present calculations.

Figure 4 shows the evolution of the external region population in time for a laser frequency $\omega = 0.24$ au where the dipole operator is described using the length gauge. Similar to the laser frequency shown in figure 2, the length-gauge description produces a highly consistent set of external region populations, with a ratio between the highest and lowest ionization probabilities of only 1.03. This range is smaller than that obtained at a frequency of $\omega = 0.33$ au which may indicate that higher lying atomic structure decreases in importance with decreasing frequency. Similarly, the highest probability is again produced when only the He^+ 1s orbital is included in the basis set. Numerical values for the final ionization probabilities are given in table 2.

Populations in the external region for the same laser frequency using the velocity-gauge description of the laser field are shown in figure 5. It is immediately apparent that

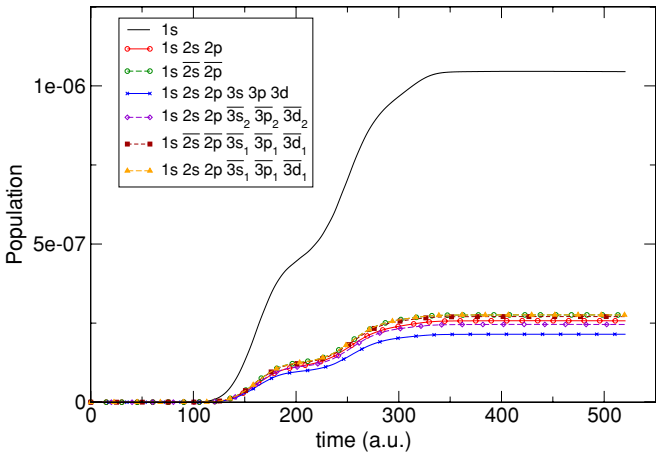

Figure 5. Population of the external region for the velocity gauge using a pulse frequency of $\omega = 0.24$ au for six cycles at a peak intensity of 2×10^{13} W cm^{-2}. Details on the basis sets used are given in the caption to figure 2.

including only the 1s state of He^+ in the basis set produces an ionization probability that is significantly higher than all others. This leads to a much larger ratio between the highest and lowest results, compared to a frequency of $\omega = 0.33$ au, of 4.87. Excluding only the 1s calculation, this ratio between the highest and lowest probabilities still amounts to 1.29. When more He^+ orbitals are included these results once again converge towards those obtained using the length gauge. However, convergence is not uniform. The ionization probability in the 1s 2s 2p 3s 3p 3d calculation lies well below the other results, including the 1s 2s 2p calculation. Numerical values for the final ionization probabilities are also given in table 2.

The ionization probabilities obtained here can be compared with those of other approaches. We have performed RMF calculations for a four-photon process using the 1s,2s,2p basis at 0.24 au and $I = 2 \times 10^{13}$ W cm^{-2}, similar to earlier work for three-photon ionization [16]. The parameters are $L_{max} = 7$, with seven absorption blocks and three emission blocks. From the obtained ionization rate of 5.05×10^7 s^{-1}, we estimate an ionization probability of 2.30×10^{-7}, about 17% less than that obtained in the present calculations. Perturbative four-photon ionization cross-sections have also been obtained [17]. These give an ionization probability which is about 50% larger than observed here. The differences between the three calculations are the same order of magnitude. The magnitude of the differences again reflects the difficulty in obtaining precise multi-photon ionization rates.

In each of figures 2–5 there is a visible oscillatory behaviour in the ionization probability during the propagation into the external region, most predominantly at a frequency of $\omega = 0.24$ au. This behaviour is due to the 1s2s ^{1}S resonance for three-photon ionization, and the 1s2p ^{1}P resonance for four-photon ionization, reached after absorption of two and three photons respectively. The detuning in the former process is about 0.1 au, leading to an oscillatory behaviour with a period of approximately 60 au. The detuning in the latter is about 0.06 au, resulting in oscillations with a period of approximately 105 au.

3.3. Discussion

Comparison of the length- and velocity-gauge results shows that for both laser frequencies, use of the length gauge provides a more consistent approximation for the ionization probabilities than the velocity gauge. This is reflected in the much lower relative range of results for the length gauge, 1.09 and 1.03, when compared with the equivalent ranges using the velocity gauge, 1.7 and 4.87. These ratios, corresponding to laser frequencies of $\omega = 0.33$ au and $\omega = 0.24$ au respectively for each gauge, also demonstrate that the consistency of the length gauge improves as the minimum number of photons involved increases from three to four whereas the consistency of the velocity gauge significantly deteriorates. However, as calculations were only performed at two frequencies further investigation is necessary before any firm conclusions may be drawn from these results.

The deterioration in consistency observed in the velocity gauge is largely due to calculations that include only the He^+ 1s orbital in the basis set. Ignoring these results, the equivalent ratio between the highest and lowest final ionization probability in the velocity gauge still increases from 1.280 for a frequency of $\omega = 0.33$ au to 1.285 for a frequency of $\omega = 0.24$ au. This is in part due to non-uniform convergence leading to fortuitous agreement between the length-gauge and the velocity-gauge calculations for the 1s,2s,2p basis, as reflected by tables 1 and 2. However, extension with the 3s, 3p and 3d states of He^+ worsens the agreement, mainly by reducing the ionization probability in the velocity-gauge calculation. Indeed, in every set of calculations it was noted that the He^+ 1s basis set produced results which agreed least with those of other larger basis sets, particularly in the velocity gauge.

As the number of He^+ states included in the basis sets was increased, the final ionization probabilities tend to converge, in particular when pseudo-orbitals are employed, for both gauges despite the higher sensitivity to the basis set in the velocity gauge. However, we also consider the effect increasing the number of basis orbitals used has on the ratio of the final ionization probability in the velocity gauge to the equivalent probability in the length gauge for a laser frequency $\omega = 0.33$ au in table 1, and $\omega = 0.24$ au in table 2. It is immediately apparent that the best agreement between the velocity gauge and length gauge occurs when we use pseudo-orbitals, particularly those with the same decay as the He^+ 1s orbital. In the latter case, differences between length- and velocity-gauge calculations amount to less than 2%.

In addition to the convergent trend within each gauge noted earlier, tables 1 and 2, also display a general convergence between the length gauge and velocity gauge ionization probabilities with the addition of orbitals and psuedo-orbitals to the basis set. In most multi-electron calculations, especially those for complex atoms, one is restricted to use a limited basis set for the atomic structure. In such a case, the length-gauge description of the dipole operator is the better choice of the two, as it will achieve a higher degree of convergence using a smaller number of final ionic states.

The observation that the use of the length gauge is preferable over the velocity gauge at first glance appears to

contradict the findings of Cormier and Lambropoulos [12]. However, it is important to realize that there are critical differences in the type of problem investigated. Cormier and Lambropoulos investigated the number of angular momenta needed to obtain converged ionization probabilities in time-dependent calculations for strong field ionization of H. They found that the number of angular momenta needed for convergence is much larger in the length gauge than in the velocity gauge. However, these calculations concerned a longer pulse with a quiver amplitude approximately a factor of 10 larger than that in the present calculations. Thus, high intensity effects were much more prominent than in the present study. On the other hand, H is a single-electron system, for which it is feasible to use an effectively complete basis set, whereas the present study investigates an explicit multi-electron problem, and, in particular, the use of a restricted basis set. For an effectively complete basis set, the length- and velocity-gauge matrix elements will be in good agreement with each other. In the case of a two-electron problem, it is possible to employ effectively complete basis sets using large-scale facilities, however, for problems involving more than two electrons, this is no longer feasible and one cannot avoid the use of restricted basis sets. In the present TDRM approach, the outer (ejected) electron is described using an effectively complete basis set, but the residual electron(s) are described using a highly restricted basis set. It is this restriction on the residual electrons that leads to the preference of the length gauge over the velocity gauge in explicit multi-electron problems. Of course, with larger quiver amplitudes the number of angular momenta that needs to be retained in the calculations is still expected to increase substantially.

In order to explain that restrictions on the movement of the inner electron may affect the choice of gauge, we can consider the general problem of the preferred gauge when a restricted basis is used. This problem was considered by Starace [21]. He considered a general configuration interaction approach, where we consider the interaction of a model Hamiltonian with a restricted set of N-electron Slater-determinant wavefunctions. As the internal region in an R-matrix approach uses such an approach [19], the analysis is considered relevant. Starace demonstrated that, given a restricted set, the configuration interaction method involves an implied non-local potential representing the interaction between the configurations being mixed. The subsequent analysis argued that, for a non-local potential, the length formula for the electric dipole matrix elements provides the correct elements. Starace further clarifies [22] that disagreement with experimental results in the length formula is due to inadequacy in the chosen approximate Hamiltonian, with the disagreement between the length and velocity formulae providing a measure of the non-locality of a potential. It is noted, however, that the work by Starace concerns primarily the accuracy of the dipole matrix elements, and as such may not fully apply to the direct solution of the time-dependent Schrödinger equation.

Another reason for the preference of the length-gauge description can be identified by examining multi-photon matrix elements. A two-photon matrix element is given by

$$M_{fi} = \sum_m \frac{\langle \Psi_f | \hat{D} | \Psi_m \rangle \langle \Psi_m | \hat{D} | \Psi_i \rangle}{E_m - (E_i + \omega)}, \tag{26}$$

where the sum over intermediate states m denotes a sum over bound states and an integral over continuum states. $\hat{D}$ is the dipole operator, and Ψ_i and Ψ_f are the initial and final states, respectively. The dipole operator can be written as

$$\hat{D} = \mathbf{E}(t) \cdot \mathbf{r} \tag{27}$$

in the length form or as

$$\hat{D} = \frac{1}{c} \mathbf{A}(t) \cdot \mathbf{p} \tag{28}$$

in the velocity gauge. The matrix elements involving a single occurrence of the dipole operator in the length form or in the velocity gauge can be linked to each other:

$$\mathrm{i}(E_f - E_m) \langle \Psi_f | \hat{\mathbf{r}} | \Psi_m \rangle = \langle \Psi_f | \hat{\mathbf{p}} | \Psi_m \rangle. \tag{29}$$

In addition, the electric field and the vector potential are related to each other by

$$\mathbf{E}(t) = -\frac{1}{c} \frac{\mathrm{d}}{\mathrm{d}t} \mathbf{A}(t), \tag{30}$$

which, for a long laser pulse at constant intensity, leads to the following relationship between the field amplitudes: $E_0 = -\omega A_0 / c$. Using these relationships, the two-photon matrix element using the length form of the dipole operator becomes

$$M_{fi} = (E_0)^2 \sum_m \frac{\langle \Psi_f | \hat{z} | \Psi_m \rangle \langle \Psi_m | \hat{z} | \Psi_i \rangle}{E_m - (E_i + \omega)}, \tag{31}$$

whereas using the velocity gauge it becomes

$$M_{fi} = -\left(\frac{E_0}{\omega}\right)^2 \sum_m \times \frac{(E_f - E_m)(E_m - E_i) \langle \Psi_f | \hat{z} | \Psi_m \rangle \langle \Psi_m | \hat{z} | \Psi_i \rangle}{E_m - (E_i + \omega)}. \tag{32}$$

The radius of the electron cloud during the two-photon transition will not change significantly, since it takes time for the electron cloud to evolve. Hence, the value of the radial matrix element will have a maximum magnitude given by the extent of the electron cloud. A comparison of the two matrix elements shows that the velocity-gauge matrix element emphasizes transitions involving a large change of energy, whereas the length-gauge matrix element emphasizes transitions near the intermediate energies. This may be seen easily through considering how an individual term of the summation for a two-photon matrix element scales with $(E_m - E_i)$ for $E_m - E_i \gg \omega$. Clearly the relevant term in the summation for a length-gauge matrix element in (31) scales approximately as $1/(E_m - E_i)$ whereas the same term in the summation for a velocity-gauge matrix element in (32) scales approximately as $(E_f - E_m)/\omega^2$. Consequently, the significance of this term in the overall summation decreases in the length gauge, and hence is less significant with respect to overall convergence of the summation, whereas in the velocity gauge the significance of the relevant term increases. Thus,

the velocity gauge requires a better description of the high-energy part of the atomic spectrum to ensure convergence in the overall summation than the length gauge.

The accurate description of the high-energy part of the spectrum is a significant problem for a general atom. In single-electron or two-electron systems, the description of the high-energy part of the atomic spectrum can be carried out reliably. However, in a general multi-electron system such a description may be unfeasible. Excitations may occur from many shells, including inner shells. Inner-shell excitations will be characterized by high energy, and their accurate description is thus crucial for the accurate determination of multi-photon matrix elements in the velocity gauge. On the other hand, the accurate description of inner-shell excitations will require enormous basis sets. For the investigations in the present study, it is thus not surprising that the ionization probabilities in the length gauge are more consistent with each other.

The difficulties in obtaining accurate matrix elements in the velocity gauge become greater when the number of photons to be absorbed increases. This can be demonstrated by examining the four-photon matrix element, which is given by

$$M_{fi} = \sum_{pqr} \times \frac{\langle\Psi_f|\hat{D}|\Psi_r\rangle\langle\Psi_r|\hat{D}|\Psi_q\rangle\langle\Psi_q|\hat{D}|\Psi_p\rangle\langle\Psi_p|\hat{D}|\Psi_i\rangle}{(E_r-(E_i+3\omega))(E_q-(E_i+2\omega))(E_p-(E_i+\omega))}. \quad (33)$$

We now envisage a transition in which absorption of the second photon leads to a state with an energy close to $E_i + 2\omega$. Transformation of the matrix element in the velocity gauge gives

$$M_{fi} = \left(\frac{E_0}{\omega}\right)^4 \sum_{pqr} \times \frac{(E_f-E_r)(E_r-E_q)(E_q-E_p)(E_p-E_i)}{(E_r-(E_i+3\omega))(E_q-(E_i+2\omega))(E_p-(E_i+\omega))} \times \langle\Psi_f|\hat{z}|\Psi_r\rangle\langle\Psi_r|\hat{z}|\Psi_q\rangle\langle\Psi_q|\hat{z}|\Psi_p\rangle\langle\Psi_p|\hat{z}|\Psi_i\rangle \quad (34)$$

in which we now have four factors of ΔE in the numerator and only two large differences in the denominator, since $E_q \approx E_i + 2\omega$. Thus, in the four-photon case, the high-energy part of the spectrum is even more strongly emphasized than in the two-photon case, leading to a slower rate of convergence relative to the number of intermediate states included for the total summation compared to the two-photon case of (32). This is of particular importance in a general multi-electron target where high energy processes such as inner-shell excitations are possible and must be described properly.

4. Conclusions

In this paper we have compared three- and four-photon ionization probabilities for He obtained using both the length- and velocity-gauge descriptions of the dipole operator within the TDRM method at a peak intensity of 2×10^{13} W cm^{-2}. In each case various basis sets are used to describe He in order to investigate the effect of atomic structure details in the basis set for each gauge. An increase in the number of final state wavefunctions included in the calculations, and in particular using pseudo-orbitals, leads to a convergent set of ionization probabilities for both gauges. The ionization probabilities are in agreement with those deduced from ionization rates and cross-sections obtained by time-independent approaches.

For both three- and four-photon ionization processes, the length gauge provides a more consistent ionization probability with respect to the atomic structure detail used in the basis set. The consistency of the length-gauge calculations increases slightly with decreasing frequency, while the velocity-gauge calculations become much more inconsistent. Hence, the length gauge appears to be less sensitive to the number of orbitals used to describe He than the velocity gauge. When additional orbitals are included in the basis set, the resulting ionization probabilities are found to converge in both gauges. Furthermore, this also causes the length- and velocity-gauge probabilities to converge towards each other, with the highest degree of agreement between gauges observed when pseudo-orbitals are included. Overall, the length gauge is the better choice for describing the dipole operator for multi-photon ionization of He due to a lower requirement for atomic structure details in the basis used.

When the complexity of the atom increases, it becomes even more important to use the length gauge. Whereas it is feasible, using massively parallel computer facilities, to describe two-electron systems in full dimensionality, for more complex atoms such as Ne, a full-dimensional treatment is not feasible. Consequently, the *ab initio* description of a general atom in an intense laser field requires the use of restricted basis sets. These restrictions will have a greater impact on the velocity-gauge calculations than on the length-gauge calculations. For example, the velocity gauge emphasizes large energy transfer, and thus, will be more sensitive to inner-shell transitions.

Acknowledgments

SH was supported by the Department of Employment and Learning NI under the Programme for Government. MAL was supported by grant no EP/E000223/1 from the UK Engineering and Physical Sciences Research Council. HWH was supported by grants EP/E000223/1 and G/055816/1 from the UK Engineering and Physical Sciences Research Council.

References

[1] Meyer M *et al* 2008 *Phys. Rev. Lett.* **101** 193002
[2] Ackermann W *et al* 2007 *Nature Photonics* **1** 336
[3] Smyth E S, Parker J S and Taylor K T 1998 *Comput. Phys. Commun.* **114** 1
[4] Parker J S, Doherty B J S, Taylor K T, Schulz K D, Blaga C I and DiMauro L F 2006 *Phys. Rev. Lett.* **96** 133001
[5] van der Hart H W, Lysaght M A and Burke P G 2007 *Phys. Rev.* A **76** 043405
[6] Lysaght M A, Burke P G and van der Hart H W 2008 *Phys. Rev. Lett.* **101** 253001

[7] Guan X, Zatsarinny O, Bartschat K, Schneider B I, Feist J and Noble C J 2007 *Phys. Rev.* A **76** 053411
[8] Guan X, Zatsarinny O, Noble C J, Bartschat K and Schneider B I 2009 *J. Phys. B: At. Mol. Opt. Phys.* **42** 134015
[9] Lysaght M A, van der Hart H W and Burke P G 2009 *Phys. Rev.* A **79** 053411
[10] Lysaght M A, Hutchinson S and van der Hart H W 2009 *New J. Phys.* **11** 093014
[11] Lysaght M A, Burke P G and van der Hart H W 2009 *Phys. Rev. Lett.* **102** 193001
[12] Cormier E and Lambropoulos P 1996 *J. Phys. B: At. Mol. Opt. Phys.* **29** 1667–80
[13] Shakeshaft R 1988 *Z. Phys.* D **8** 47–50
[14] Burke P G, Francken P and Joachain C J 1991 *J. Phys. B: At. Mol. Opt. Phys.* **24** 761–90
[15] Robicheaux F, Chen C-T, Gavras P and Pindzola M S 1995 *J. Phys. B: At. Mol. Opt. Phys.* **28** 3047–62
[16] van der Hart H W and Bingham P 2005 *J. Phys. B: At. Mol. Opt. Phys.* **38** 207–21
[17] Saenz A and Lambropoulos P 1999 *J. Phys. B: At. Mol. Opt. Phys.* **32** 5629
[18] Burke P G and Burke V M 1997 *J. Phys. B: At. Mol. Opt. Phys.* **30** L383
[19] Burke P G and Berrington K A 1993 *Atomic and Molecular Processes: An R-Matrix Approach* (Bristol: Institute of Physics Publishing)
[20] Dörr M, Terao-Dunseath M, Purvis J, Noble C J, Burke P G and Joachain C J 1992 *J. Phys. B: At. Mol. Opt. Phys.* **25** 2809–29
[21] Starace A F 1971 *Phys. Rev.* A **3** 1242–5
[22] Starace A F 1973 *Phys. Rev.* A **8** 1141–2